Heliyon 10 (2024) e36114

Contents lists available at ScienceDirect

Heliyon

journal homepage: www.cell.com/heliyon

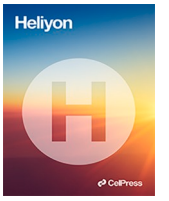

Research article

Thermoelectric bismuth telluride nanostructures fabricated by electrodeposition within flexible templates

P. Cervino-Solana , M.J. Ramirez-Peral , M.S. Martín-González , O. Caballero-Calero *

Instituto de Micro y Nanotecnología, IMN-CNM, CSIC (CEI UAM+CSIC) Isaac Newton, 8, E-28760, Tres Cantos, Madrid, Spain

A R T I C L E I N F O

Keywords:
Thermoelectricity
Electrodeposition
Bismuth telluride
Nanostructures

A B S T R A C T

Bismuth telluride, a highly efficient thermoelectric material, stands out for applications around room temperature in wearable devices. By harnessing the thermal gradient established between the human body and ambient temperature, we can generate useable electricity. Notably, bismuth telluride nanostructures exhibit significantly lower thermal conductivities compared to their bulk counterparts. As a result, the thermoelectric efficiency achieved is notably higher. Our research focuses on developing efficient nanostructured materials based on bismuth telluride inside a flexible substrate made of polyester. We employ scalable methods, such as template-assisted electrochemical deposition, to fabricate these nanostructures. In this study, we present an approach to the development of flexible nanostructured thermoelectric materials. Despite using a reduced quantity of active material, our electrochemically deposited nanostructures inside a flexible template demonstrate a remarkable performance. They exhibit 24 % of the Power Factor reported for conventional electrochemically fabricated Bi_2Te_3 thin films, and notably, they even surpass the Power Factor reported for flexible Bi_2Te_3-based inks used in the creation of flexible generators. This achievement underscores the potential of our method in the advancement of efficient, flexible thermoelectric devices.

1. Introduction

Bismuth telluride (Bi_2Te_3) stands out as a reference thermoelectric material for room-temperature applications, that is, to convert thermal gradients into useable electric voltage. In such a way, wasted heat produced around room temperature, such as that produced by the human body, in buildings, or many other sources of heat in our daily lives, can be converted into useable electrical power [1]. In this context, Bi_2Te_3 which has its maximum thermoelectric efficiency around room temperature, is quite an interesting material for energy recovery. This efficiency is related to the thermoelectric Figure of Merit, which is expressed as $ZT = S^2 \cdot \sigma \cdot T \cdot \kappa^{-1}$, where S the Seebeck coefficient, σ the electrical conductivity, T the absolute temperature, and κ the thermal conductivity. Then, the higher the numerator, and the lower the denominator (that is, κ) the better the thermoelectric performance.

Bi_2Te_3 fabrication via electrochemical deposition was first reported in 1993, and it has been widely used ever since [2–4]. Electrodeposition has many advantages over other techniques, such as being a cost-effective method widely used in industry that does not require vacuum or expensive facilities to be used. This method to obtain Bi_2Te_3 has been thoroughly studied, from the electrodeposition method itself [5] to the effect that different deposition techniques [6–8] or additives [9–11] have on the final properties of the material [12]. Also, current research on this field is exploring the fabrication of Bi_2Te_3 supperlattice structures [13], how to measure

* Corresponding author.
E-mail address: olga.caballero@csic.es (O. Caballero-Calero).

https://doi.org/10.1016/j.heliyon.2024.e36114
Received 3 April 2024; Received in revised form 24 July 2024; Accepted 9 August 2024
Available online 10 August 2024

thermoelectric properties in electrodeposited films (avoiding the influence of the conductive substrate necessary for the electrochemical growth) [14,15] or the influence of changes in the electrolyte on their final performance [16,17].

More recently, the fabrication of nanowires of Bi_2Te_3 mainly via template-assisted electrochemical deposition inside polycarbonate membranes [18,19] or anodic alumina templates [20,21] has also been of great interest. In the latter case, several studies from our group showed that the thermal conductivity of Bi_2Te_3 nanowires [22] decreases when reducing the nanowire radius [23]. This thermoelectric enhancement at low dimensions, along with the fact that Bi_2Te_3 is a topological insulator, has also triggered further studies in this material [24] and, more precisely, in nanostructures fabricated with Bi_2Te_3 [25,26].

More recently, thanks to the development of interconnected nanoporous structures fabricated in anodic alumina templates, so-called 3D anodic aluminum oxide (AAO) templates [26,27] have allowed the implementation of a novel 3D Bi_2Te_3 nanostructure, which consists of 50 nm diameter nanowires connected to their first neighbors by transversal nanowires of 30–40 nm diameter. These structures are also obtained by template-assisted electrochemical deposition (using the 3D-AAOs as templates) [28]. These 3D Bi_2Te_3 nanostructures present a further reduction of the κ when compared to conventional Bi_2Te_3 nanowires [29], and many interesting effects are being found in them, such as plasmon resonances modified from the ones found in Bi_2Te_3 bulk and Bi_2Te_3 nanowires [30] or modified transport due to the topologically insulating nature of their surface [31]. Then, it seems that not only the dimensions themselves, that is, achieving sizes of tens of nanometers in diameter, but also the interconnection of the structures, play an important role in the behaviour of Bi_2Te_3 at the nanoscale.

This work presents an alternative way of obtaining interconnected nanostructures with a scalable and cost-effective method: template assisted electrochemical deposition inside commercial nanoporous polyester filters. The process of making the nanostructured material is similar to the process used to make Bi_2Te_3 nanowires or 3D-Bi_2Te_3 nanowire networks inside AAOs or 3D-AAOs, respectively, but the use of polyester filters adds a novel feature to the fabricated nanostructured material, which is flexibility. This will allow the use of this material as the active part on flexible wearable thermoelectric generators. The current research in this field is quite relevant, as it can be seen in recent reviews on the subject [32–34]given that it will provide a way of powering sensors, microelectronics based devices, etc. that will convert the body heat of the person wearing them into useable electricity, mainly using small and flexible thermoelectric devices [35]. Among the different thermoelectric materials studied for this application, Bi_2Te_3 stands out as one of the main candidates, provided it can be fabricated in the form or inks [36–40], by sputtering thin films on flexible substrates [41], or, as we show here, embedded in flexible polymeric matrices. In our work, the actual Bi_2Te_3-fabricated nanostructures embedded in the polyester filter consist of interconnected nanowire-like cylinders of around 200 nm in diameter. The optimization of the fabrication of these structures, filling the nanoporous structure completely with the highest Power Factor will be described in this work.

2. Experimental

2.1. Fabrication methods

The templates used were commercial polyester nanoporous filters (from Sterlitech Corp., with cylindrical pores of 200 $\pm$ 20 nm in diameter and a total thickness of 10 μm and a diameter of 130 mm). One of the template faces was electron-beam evaporated with 5 nm of chromium and 150 nm of gold.

Electrochemical processes were performed with a potentiostat/galvanostat from Autolab (model PGSTAT302N) controlled with the software Nova 2.0. The electrochemical deposition of gold was made in a two-electrode cell, with the working electrode (WE) the afore-mentioned template with the evaporated chromium and gold layers exposed to the electrochemical bath and electrically connected to a copper holder by silver paint, and the counter electrode (CE) being a platinum mesh. In this case, the electrochemical solution consists of a gold sulphite commercial plating solution with 15 Au/l (Gold–SF–bath from Metakem GmbH).

For the electrodeposition of Bi_2Te_3, a standard three-electrode cell was used. In this case, the WE consists of the polyester template with the uncoated surface facing the electrochemical bath, which was maintained at 0 °C. To form the WE, the conductive layers were connected via silver paint to a copper holder. The exposed areas of both the copper holder and the polyester template borders were covered with non-conductive lacquer to prevent deposition in these areas. The CE was again a platinum mesh, and the reference electrode (RE) is an Ag/AgCl in saturated KCl electrode. The solution used was the same optimized in our group for the electrodeposition inside alumina templates [23,28], that is, 10^{-2} M $HTeO_2^+$ (tellurium powder ~30 msh 99.997 % from Sigma Aldrich), $0.907{\cdot}10^{-2}$ M Bi^{3+} (bismuth pieces 1–12 mm size, 99.999 % Aldrich Chemistry), and 1 M HNO_3 (nitric acid, 65 % from J. T. Baker) in de-ionized water. To this solution, 0.045 g/l of sodium lignosulfonate (SLS, lignosulfonic acid, sodium salt, from Aldrich) were added. This surfactant additive has been shown to improve the performance of Bi_2Te_3 thin films [9] and has also had an influence on the morphology of the electrodeposited films.

2.2. Characterization methods

The samples were cut with standard scissors to perform side-views of the morphology of the nanostructure, which were studied with a high-resolution Scanning Electron Microscope (SEM) from FEI (model Verios 460). Two main detectors were used, the trough lens detector (TLD) which recoils secondary electrons and gives information about the morphology of the sample, and the mirror detector (MD), which recoils back scattered electrons and is sensitive to the composition, appearing lighter in areas with higher electrical conductivity (the Bi_2Te_3 and conductive layers in our case) than the non-conductive regions (for us, the polyester template). The composition of the samples was obtained by Electron Dispersive X-ray (EDX) analysis in a JEOL JSM6335F SEM (a service from the SIdI – Servicio Interdepartamental de Investigación-, in the Universidad Autónoma de Madrid). The crystallographic orientation of the

samples was measured by an X-Ray diffractomter from Bruker (model D8 Discover) which has an X-Ray microsource and a 2D Eiger 2 detector. Raman spectra were collected with a MicroRaman system from Horiba (confocal micro-Raman system model Jobin Yvon LabRAM 800) with a Nd:YAG laser (532 nm) of incident wavelength.

The Power Factor ($PF = S^2 \cdot \sigma$, being S Seebeck coefficient and σ electrical conductivity) around room temperature (RT) were characterized with systems adapted to the measurement of thin films, given that the Bi_2Te_3 nanostructures are interconnected and are electrically conductive in the in-plane direction, as it will be explained later. Seebeck coefficient (S) was obtained by a lab-made setup where both, a temperature gradient established around room temperature (established between two Peltier modules and measured with two thermocouples), and the voltage produced by this gradient (measured with two iron tips). The temperatures given by thermocouples and the voltage drop are measured by a Keithley 2000 Multimeter. The coefficient between the voltage and the gradient results in the S value. By varying the voltage applied to two Peltier modules, the measurement can be performed at different temperature gradients around room temperature. The electrical conductivity (σ) has been measured in a four-probe van der Pauw configuration with an electronic transport measuring system from Ecopia (model HMS-550).

In the cases where the bottom gold electrode had to be selectively etched for different electrical measurements, different methods were tested. The first essays were made by completely removing the gold layer with chemical etching (such as using I_2-KI solutions), but then it was quite complicated to make electrical contact between the macroscopic tips for electrical measurements and the nanostructure, which is embedded in the polyester filter. Then, a different approach was taken, which was to selectively etch mechanically the gold in certain regions with alumina powder and leave others to make electrical contact with the electrochemically grown nanostructure. To that end, the sample was fixed with wax to a steel polishing jig and alumina powders of different diameters (3 μm and 1 μm) were used. For the electrical transport measurements, two stripes were mechanically polished away on the bottom gold electrode. The initial stripe leaved two areas with electrically good gold contacts, as can be seen in Fig. 1a. And then, a second stripe were polished, as can be seen in Fig. 1b, so the electrical conductivity could be measured in a van der Pauw configuration using four electrical probes. To confirm that after this process, the gold was completely removed from the central area of the sample, SEM images of the surface were taken (Fig. 1c shows approximately the region marked in Fig. 1b with a square). There, the gold is completely removed, and even the bottom of the Bi_2Te_3 nanostructures can be seen in the polished region. Then, we grant that the only way to have contact between two gold electrodes is through the Bi_2Te_3 nanostructure.

3. Results and discussion

3.1. Fabrication and optimization of the Bi_2Te_3 nanostructures

First attempts were made to electrodeposit Bi_2Te_3 inside commercial nanoporous polyester filters in the three-electrode configuration cell mentioned above, which is the WE commercial filter coated with 5 nm chromium and 150 nm gold layers. These layers were brought into electrical contact with a copper holder using silver paint. The electrodeposition area was defined by non-conductive lacquer. Before carrying out the electrodeposition processes, Cyclic Voltammetries (CVs) were performed to identify the applied voltages *vs.* Ag/AgCl at which the reduction peak takes place. CV was done by varying the applied voltage *vs.* Ag/AgCl at 10 mV s^{-1} rate from the Open Circuit Potential (OCP) to −0.3 V, then increasing up to +0.8 V and finishing again at the OCP. The first CVs made on different commercial polyester filters showed that it was necessary to always perform the CV because the position and intensity of the reduction peak changed with each sample. Then, once the reduction peak was characterized, a pulsed electrodeposition process was carried out, consisting of pulses with two steps: a deposition step and a relaxation step. During the deposition step, for a certain t_{on} time, a voltage (V_{app}) is applied between the working and reference electrodes, corresponding to the voltage of the half maximum of the reduction peak obtained in the CV. For the relaxation step, during a certain time (t_{off}) a zero-current condition is set in the bath. The relaxation step is essential to prevent the shrinkage of the concentration of $HTeO_2^+$ and Bi^{3+} ions near the working electrode. This process is analogous to that employed in previous works by the group for the template-assisted growth of Bi_2Te_3 inside anodic aluminum [23,24,28]. After trying different t_{on} and t_{off}, the best results were obtained with pulses of t_{on} of 1 s and t_{off} of 0.1 s, which are similar to those used for the filling of the 3D anodic aluminum templates [28]. This resulted in the conformal filling of the cylindrical pores of the polyester filter with Bi_2Te_3.

Nevertheless, the observed filling ratio was quite low, and it did not increase regardless of the electrodeposition parameters employed. After some trials with different times, pulses, etc. we realized that the surface of the nanoporous polymer filters (see Fig. 2a)

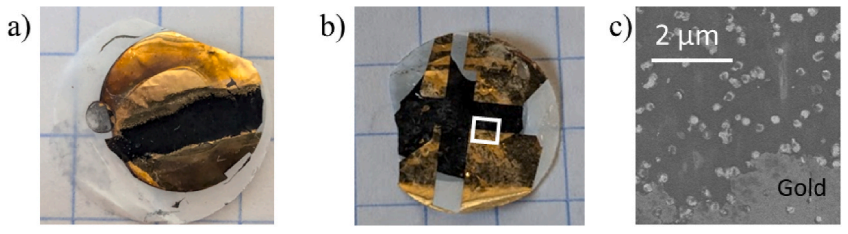

Fig. 1. a) sample with two gold contacts left after polishing the bottom gold electrode for Seebeck measurements, b) sample with four contacts left after a second step of polishing, for electrical conductivity measurements c) SEM images of the surface of the sample after polishing away the gold layer.

was not completely covered by the electron-beam-deposited chromium and gold layers, and in the SEM images, the surface showed a certain number of open pores (Fig. 2b). Even when the deposited gold layer thickness was increased to 200 nm (Fig. 2c) the covering of the nanopores was not complete. That explained, on the one hand, the low reproducibility of the CV, given that part of the solution was going through the filter, making contact with the silver paste or even the copper holder. On the other hand, the low filling ratio (see Fig. 2d) and the difficulties in filling the whole template could also be since the WE were not homogeneous everywhere, but the non-closed pores were not acting as electrochemical cells, and therefore, Bi_2Te_3 could not grow inside them.

Then, we had to optimize the working electrode, because it was clear that the low reproducibility and low filling ratio were a consequence of the poor covering of the pores with the conductive gold layer. The first approach to solving this problem consisted of chemically electrodepositing nickel on the gold layer to obtain a complete covering of the pores. These trials showed that, although the deposit of nickel was successful, the problem reappeared when performing the subsequent Bi_2Te_3 deposit. The reason was that nickel is attacked by the electrochemical bath used for the growth of Bi_2Te_3, which contains 1 M HNO_3, and therefore the electrodeposited nickel used for the covering of the pores was completely removed in the subsequent immersion in the Bi_2Te_3 electrochemical bath.

Therefore, we chose a material for the covering of the pores that was not etched with the electrochemical bath. In consequence, the electrodeposition of gold on the previously evaporated gold layer was performed. In this case, first trials were made by performing the electrochemical deposit of the gold layer with the same disposition as for the filling of the pores. This configuration has the advantage that the WE does need to be dismounted for the later Bi_2Te_3 deposition. But we observed that when the gold electrodeposition was performed through the nanopores, the employed electrochemical bath solution left such an amount of debris that it was impossible to carry out any later Bi_2Te_3 chemical electrodeposition. Therefore, we decided to introduce a previous step, which consisted of placing the rear-side of the nanopores covered with the evaporated gold layer in direct contact with the solution. Then, the contact of the gold layer with the copper holder was done with silver paint and then covered with non-conductive lacquer and the electrochemical deposit of gold was performed on the previously evaporated gold layer. After several trials with different deposit times, the parameters for the complete covering of the porous surface was achieved (see Fig. 2e).

When this first step was implemented, it was necessary to dismantle the previous WE used for gold deposition (by immersion in acetone to detach it from the copper holder, dissolving both the non-conductive lacquer and the silver paint). Then, the WE was remounted, turning the filter upside down, being the gold of the rear side, now in electrical contact with the copper holder by silver paint, and the rest of the holder and the borders of the filter covered with non-conductive lacquer to force the deposition to take place inside the filter cylindrical pores. Once this first step of gold electrodeposition was set up, the cyclic voltammetry tests that were done on different commercial polyester filters were always identical and could be repeated. Moreover, the filling rate of the nano-porous structure with Bi_2Te_3 significantly increased when compared to the previous experiments without the gold electrodeposition layer (see Fig. 2f).

With this fabrication method, the conformal filling of the polyester membrane could be controlled to reproduce the porous structure, obtaining nanowire-like structures of around 200 nm in diameter that are randomly interconnected (see Fig. 2g and h). Adding sodium lignosulfonate makes the surfaces smooth, which in turn helps the nanoporous structure fill up in a conformal way. In order to optimize the electrochemical deposition, there are several parameters that can be tested. For instance, the times used for the pulsed deposition have a clear influence in the front growth of the structure, and the temperature of the bath influences how fast the structures grow. Given that the temperature of the bath and the pulses chosen from our experience in filling anodic alumina templates of similar pore diameters (t_{on} of 1 s and t_{off} of 0.1 s) gave rise to a homogeneous front in the whole membrane, these parameters were not changed. Another parameter that is important to optimize the material grown is the applied voltage. It is clear that for obtaining Bi_2Te_3 the voltage applied *vs.* Ag/AgCl has to be within the ranges of the voltages at which the reduction peak of the cyclic voltammetry appears. The different applied voltages result in different Bi/Te rates. Therefore, we tested different voltages for the

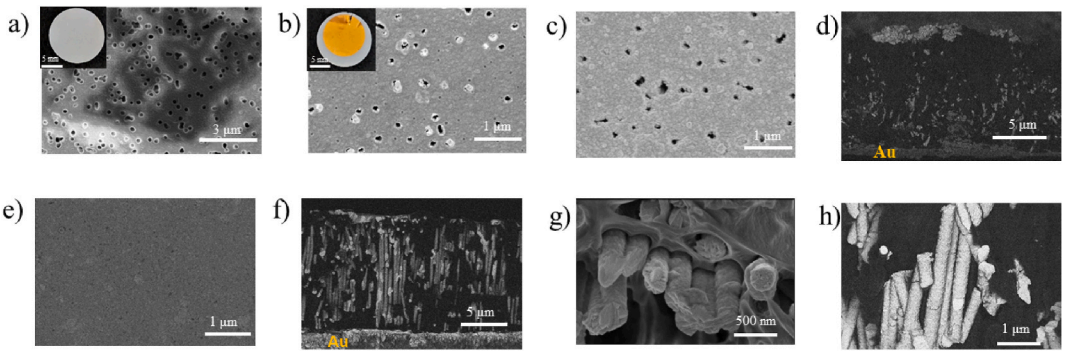

Fig. 2. a) SEM image of the nanoporous surface of a commercial polyester filter as purchased (shown in a photo in the inset), and b) with the conductive layer (the inset shows a photo of a sample at this stage), showing that some of the nanopores has not been covered after electron-beam evaporation of 5 nm Cr and 150 nm Au or c) higher thicknesses of gold. d) compositional sensitive SEM image of a lateral view of filter with electron-beam deposited conductive layer after electrodeposition of Bi_2Te_3. Gold and bismuth telluride appear lighter, and it can be seen that the filling rate is quite low. e) SEM image of the surface of a commercial polyester filter after the Cr and Au electron-beam deposition and electrochemical deposition of gold. No open pores can be found. f) Compositional sensitive SEM image of a filter prepared as in e) where the complete filling of the membrane can be observed. g) and h) show details of the nanowire-like structures, with secondary (g) and backscattered (h) electrons.

electrochemical deposition of Bi_2Te_3, and the resulting samples had different compositions, which were measured by EDX (with an associated uncertainty of around 5 %). X-Ray diffraction spectra were also measured, obtaining peaks that corresponded to the Bi_2Te_3 tabulated values, according to the Crystallographic Open Database (COD) 90212064. When measuring the Raman spectra, there was a clear difference based on how the different bismuth telluride nanostructures were put together. For the samples that showed stoichiometric composition (Bi_2Te_3), the Raman spectra showed the peaks corresponding to Bi_2Te_3, that is, E_g^1, A_{1g}^1, E_g^2 and A_{1g}^2 at around 36.5, 62.0, 102.3, and 134.0 cm^{-1}, respectively [42]. But for samples with higher content of tellurium, two extra peaks at around 122 and 142 cm^{-1} could be found (corresponding to the Te vibrational modes A^1 and E^2 [43,44], as it also happened for Te-rich Bi_2Te_3 [20] nanowires), and in those with bismuth excess, the peaks corresponding to the vibrational modes E_g (65 cm^{-1}) and A_{1g} (91 cm^{-1}) could be found [42]. Examples of how the Raman spectra vary with different compositions can be found in Fig. 3. Then, this final optimization of the material growth was the study of the applied voltage and the resulting stoichiometry of the samples, choosing for further applications the compositions that gave the best thermoelectric performance.

3.2. *Power factor optimization of the Bi_2Te_3 nanostructures*

Given that the obtained nanostructure is formed by connected nanowires, as was shown in the previous section, one can measure the transport properties, that is, the Seebeck coefficient, S, and electrical conductivity, σ, in the in-plane direction in the same way that if the sample was a thin film. This greatly simplifies the characterization because, for instance, macroscopic electrical contacts and thermal gradients can be used. Nevertheless, one thing must be considered, which is the conductive layer that was used as the bottom contact for the electrochemical deposition. As it was explained in the experimental section, if the measurements are going to be carried out in the in-plane direction, the gold layer must be removed, because otherwise, we will be measuring it instead of the Bi_2Te_3 nanostructure.

To measure S, a strip of the gold layer was mechanically removed, and then a thermal gradient was established between both gold contacts, measuring the actual temperature and the voltage drop between them. The results of the measurement of the Seebeck coefficient are shown in Fig. 4a, as a function of the composition, shown as $Bi_xTe_{(5-x)}$. Thus, samples with $x = 2$ present the stoichiometric composition Bi_2Te_3, and those with $x > 2$ or $x < 2$ correspond to bismuth or tellurium rich samples. It can be seen that the highest values obtained, of ~ -100 $\mu V\ K^{-1}$ are found for samples with compositions close to the stoichiometric one, with x close to 2, that is, Bi_2Te_3. This value is almost twice that reported at room temperature for electrodeposited thin films [45], and it is similar to the value found for 3D Bi_2Te_3 nanostructures [29], which is among the best Seebeck coefficients values reported for electrodeposited Bi_2Te_3.

As it was explained before, the measurement of the electrical conductivity of the nanostructures in the in-plane direction was made after mechanically polishing another part of the bottom electrode. The electrical conductivity showed a clear trend, with the highest electrical conductivities found for those samples with compositions closer to the stoichiometry of Bi_2Te_3, with conductivities as high as

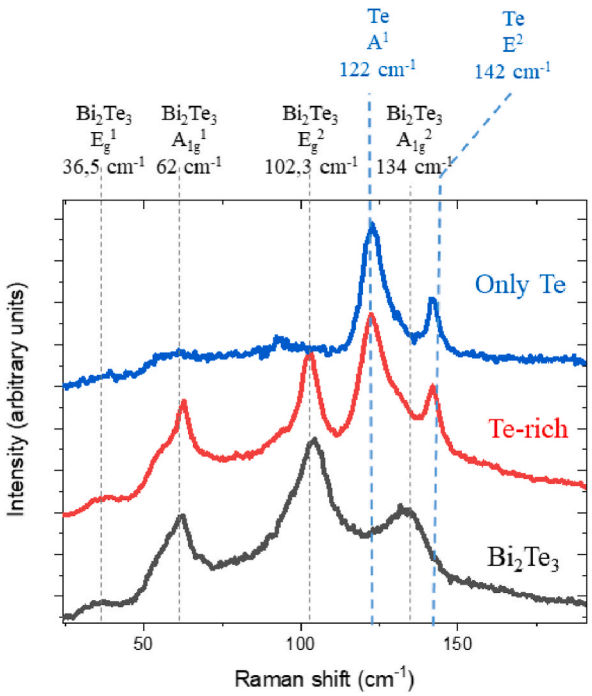

Fig. 3. Raman spectra of a stoichiometric Bi_2Te_3 nanostructure (black, lower graph), a Te-rich nanostructure (red, medium graph) and a Te nanostructure, all grown inside commercial polyester templates. The values of the different Raman modes of the literature for Bi_2Te_3 [42] and Te [43-44]and are shown as dashed lines in the picture and labelled in the top of the graph.

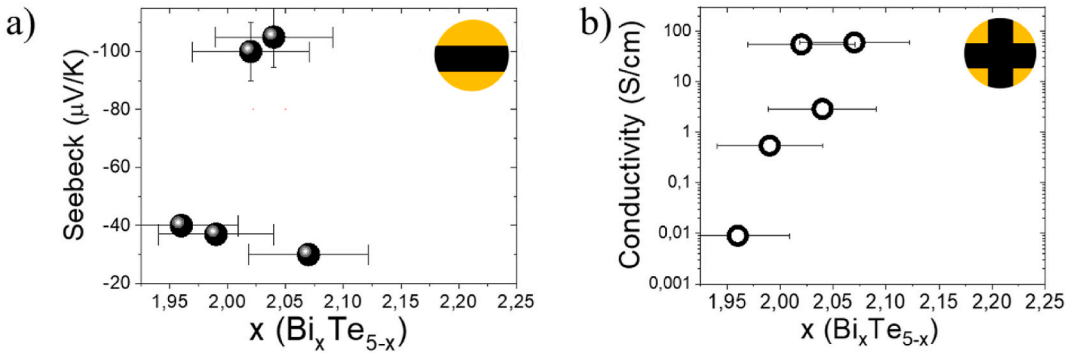

Fig. 4. a) Seebeck coefficient and b) electrical conductivity as a function of the composition of the bismuth telluride nanostructure, being the stoichiometric Bi_2Te_3 that of x = 2. x > 2 and x < 2 correspond to bismuth and tellurium rich, respectively. In both graphs, the insets show a schematic of the configuration of the remaining bottom gold electrode sample for each of the measurements.

~60 S cm^{-1} (see Fig. 4b). When compared to reported values for Bi_2Te_3 thin films (670 S cm^{-1}, in Ref. [45]) or 3D Bi_2Te_3 nanostructures (700–1000 S cm^{-1} in Ref. [29]), the obtained values in this work are around one order of magnitude lower. But taking into account the randomness of the interactions between the nanowire-like structures inside the polyester template, and the fact that the final aim of these Bi_2Te_3 nanostructures would be applications in the out-of-plane direction (where the conductivity should be higher, given that they were grown via electrochemical deposition and in that direction the structures are continuous), one can take this value as a minimum reference.

Then, if we calculate the maximum Power Factor for the stoichiometric samples with the obtained in-plane *S* at RT and the in-plane σ, it results in ~60 μW m^{-1} K^{-2} at RT. In the case of bulk single crystalline bismuth telluride, the reported Power Factor is of ~1000 μW m^{-1} K^{-2} at RT, but there is no point in comparing our samples with this value. Instead, our obtained *PF* should be compared to the reported *PF* of Bi_2Te_3 films fabricated via electrochemical deposition in similar conditions to our nanostructures, where values of ~250 μW m^{-1} K^{-2} at 50 °C [10] have been reported. It is worth mentioning that there were previous works in our group in which values as high as 500 μW m^{-1} K^{-2} at 70 °C were reported [8], but these high values were later related to impurities present in the tellurium used then [10], which is no longer available and could not be reproduced. Also other groups have reported Power Factor values for electrodeposited Bi_2Te_3 films of 1473 μW m^{-1} K^{-2} [46]. But again, the comparison of our nanostructures with these films is not straightforward, given that we do not know the kind of impurities present in those films or the reason of such a high *PF*. Other nanostructures based in template-assisted electrodeposition, such as the 3D-nanowire structures mentioned before, have been prepared within our group, with values as high as 1440 μW m^{-1} K^{-2} of *PF* reported for those with periods of 220 nm (other periods showed lower *PF*s, of 1100 or 700 μW m^{-1} K^{-2} for periods of 720 and 346 nm respectively [29]) but these structures lack flexibility and their implementation requires the fabrication of the 3D template, which makes it more complicated than directly using commercial templates as it is done in this work.

Then, to evaluate the performance of our flexible nanostructured Bi_2Te_3 material, we could compare them with other power factors obtained in electrochemically grown samples, where reported values of *PF* as high as 1100 μW m^{-1} K^{-2} when the sample is grown on top of a sputtered Bi_2Te_3 film can be found [15]. But if one compares with standard electrochemically grown Bi_2Te_3 samples, values of 336 μW m^{-1} K^{-2} were reported this year when grown on stainless steel [17] or 88 μW m^{-1} K^{-2} when grown from non-aqueous solutions [47]. Nevertheless, the correct comparison has to be done with the *PF* of films grown by electrochemistry with similar conditions, that is, those electrodeposited Bi_2Te_3 films in our group, which present reproducible *PF*s ~250 μW m^{-1} K^{-2} at 50 °C [10]. Firstly, one has to take into account that our value has been measured at RT, and the reported ones, at 50 °C, where both *S* and σ in Bi_2Te_3 are higher. But even if we do not take into account the different temperatures for the reported values, what we have is a *PF* of around 24 % that of a continuous film. But one of the advantages of the fabricated Bi_2Te_3 nanostructures is their lower content in active material, being only around 10 % of the sample actually Bi_2Te_3. Also, one could compare the obtained *PF* values with other large scale techniques like for flexible Bi_2Te_3-based inks, where *PF* of 34 μW m^{-1} K^{-2} [37] or 40 μW m^{-1} K^{-2} [36] which have been recently reported for as-printed materials (without further annealings or thermal treatments).

Therefore, these nanostructures show quite competitive values for developing future thermoelectric generators for wearable applications, given that they maintain the flexibility of the polyester commercial filter and reduce the use of bismuth and tellurium.

4. Conclusions

In this study, we present a novel interconnected nanostructure of Bi_2Te_3, which demonstrates competitive output performance. The fabrication process involves template-assisted electrochemical deposition within commercial nanoporous polyester templates. Notably the addition of sodium lignosulfonate to the electrochemical bath improved the morphology of the material, allowing a conformal growth within the porous structure. The actual amount of thermoelectric material used is only approximately 10 % of what would be required for a continuous films of the same thickness. Despite the reduced material quantity, the resulting nanostructures exhibit a remarkable 24 % of the Power Factor reported for electrochemically fabricated Bi_2Te_3 thin films and even exceed the Power Factor

reported for flexible Bi_2Te_3 based inks used to make flexible generators. This improvement underscores the effectiveness of our approach. The Bi_2Te_3 nanostructures are electrically conductive in the in-plane direction, allowing the films to be measured by techniques commonly used for thin films. This facilitates the study of their transport properties. Our fabrication method relies on scalable techniques, making it feasible to consider these nanostructures as active materials for flexible thermoelectric devices operating at room temperature. In conclusion, our work introduces a promising route to obtain a Bi_2Te_3 nanostructure embedded in a flexible polymeric membrane. These findings pave the way for practical applications in energy harvesting for wearables devices.

CRediT authorship contribution statement

P. Cervino-Solana: Writing – review & editing, Investigation, Data curation. **M.J. Ramirez-Peral:** Investigation, Data curation. **M. S. Martín-González:** Writing – review & editing, Supervision, Conceptualization. **O. Caballero-Calero:** Writing – review & editing, Writing – original draft, Validation, Supervision, Resources, Project administration, Methodology, Investigation, Funding acquisition, Formal analysis, Data curation, Conceptualization.

Declaration of competing interest

The authors declare that they have no known competing financial interests or personal relationships that could have appeared to influence the work reported in this paper.

Acknowledgements

This work has been supported by the Ramon Areces Foundation through the micro-TENERGY project. The authors would like to acknowledge the service from the MiNa Laboratory at IMN, and its funding from CM (project SpaceTec, S2013/ICE2822), MINECO (project CSIC13-4E-1794), and EU (FEDER, FSE). We also acknowledge the funding by the MINECO under grant number PID2020-118430 GB-100. O.C–C would also like to acknowledge fruitful discussions with David López Romero and the assistance with the SEM microscope from Raquel Álvaro Bruna.

References

[1] V. Pecunia, S.R.P. Silva, J.D. Phillips, E. Artegiani, A. Romeo, H. Shim, J. Park, J.H. Kim, J.S. Yun, G.C. Welch, Roadmap on energy harvesting materials, J. Phys.: Materials 6 (4) (2023) 042501.
[2] M. Takahashi, Y. Oda, T. Ogino, S. Furuta, Electrodeposition of Bi-Te alloy films, J. Electrochem. Soc. 140 (9) (1993) 2550–2553.
[3] C. Boulanger, Thermoelectric material electroplating: a historical review, J. Electron. Mater. 39 (9) (2010) 1818–1827.
[4] R. Rostek, N. Stein, C. Boulanger, A review of electroplating for V–VI thermoelectric films: from synthesis to device integration, J. Mater. Res. 30 (17) (2015) 2518–2543.
[5] M.S. Martin-Gonzalez, A.L. Prieto, R. Gronsky, T. Sands, A.M. Stacy, Insights into the Electrodeposition of Bi[sub 2]Te[sub 3], J. Electrochem. Soc. 149 (11) (2002) C546–C554.
[6] V. Richoux, S. Diliberto, C. Boulanger, J. Lecuire, Pulsed electrodeposition of bismuth telluride films: influence of pulse parameters over nucleation and morphology, Electrochim. Acta 52 (9) (2007) 3053–3060.
[7] S. Diliberto, V. Richoux, N. Stein, C. Boulanger, Influence of pulsed electrodeposition on stoichiometry and thermoelectric properties of bismuth telluride films, Phys. Status Solidi 205 (10) (2008) 2340–2344.
[8] C.V. Manzano, A.A. Rojas, M. Decepida, B. Abad, Y. Feliz, O. Caballero-Calero, D.-A. Borca-Tasciuc, M. Martin-Gonzalez, Thermoelectric properties of Bi 2 Te 3 films by constant and pulsed electrodeposition, J. Solid State Electrochem. 17 (7) (2013) 2071–2078.
[9] O. Caballero-Calero, P. Díaz-Chao, B. Abad, C.V. Manzano, M. Ynsa, J. Romero, M.M. Rojo, M.S. Martín-González, Improvement of bismuth telluride electrodeposited films by the addition of sodium lignosulfonate, Electrochim. Acta 123 (2014) 117–126.
[10] C.V. Manzano, B. Abad, M. Martín-González, The effect of electrolyte impurities on the thermoelectric properties of electrodeposited Bi2Te3 films, J. Electrochem. Soc. 165 (14) (2018) D768.
[11] M.A. Alias, K.F. Samat, N. Mohamed, M.W. Abd Rashid, M.A. Azam, N. Van Toan, T. Ono, A. Klimkowicz, A. Takasaki, Electrodeposited bismuth telluride nanocomposite thermoelectric film with improved graphene deposition, Journal of Advanced Research in Applied Mechanics 111 (1) (2023) 161–172.
[12] C.V. Manzano, B. Abad, M.M. Rojo, Y.R. Koh, S.L. Hodson, A.M.L. Martinez, X. Xu, A. Shakouri, T.D. Sands, T. Borca-Tasciuc, Anisotropic effects on the thermoelectric properties of highly oriented electrodeposited Bi2Te3 films, Sci. Rep. 6 (2016).
[13] A. Bakavets, Y. Aniskevich, O. Yakimenko, J.H. Jo, E. Vernickaite, N. Tsyntsaru, H. Cesiulis, L.-Y. Kuo, P. Kaghazchi, G. Ragoisha, Pulse electrodeposited bismuth-tellurium superlattices with controllable bismuth content, J. Power Sources 450 (2020) 227605.
[14] J. Recatala-Gomez, P. Kumar, A. Suwardi, A. Abutaha, I. Nandhakumar, K. Hippalgaonkar, Direct measurement of the thermoelectric properties of electrochemically deposited Bi2Te3 thin films, Sci. Rep. 10 (1) (2020) 17922.
[15] O. Norimasa, M. Takashiri, In-and cross-plane thermoelectric properties of oriented Bi2Te3 thin films electrodeposited on an insulating substrate for thermoelectric applications, J. Alloys Compd. 899 (2022) 163317.
[16] V.S. Khairnar, A.N. Kulkarni, V.V. Lonikar, A.B. Gite, M. Kumar, D.P. Patil, D.P. Kadam, Electrodeposition of Bi2Te3 thin films for thermoelectric applications: effect of electrolyte pH, J. Mater. Sci. Mater. Electron. 34 (10) (2023) 875.
[17] V.S. Khairnar, A.N. Kulkarni, V.V. Lonikar, N.D. Jadhav, D.P. Patil, A.B. Gite, M. Kumar, Effect of concentration of electrolyte on thermoelectric properties of electrodeposited Bi2Te3 thin films, J. Mater. Sci. Mater. Electron. 35 (19) (2024) 1–15.
[18] C. Frantz, N. Stein, Y. Zhang, E. Bouzy, O. Picht, M. Toimil-Molares, C. Boulanger, Electrodeposition of bismuth telluride nanowires with controlled composition in polycarbonate membranes, Electrochim. Acta 69 (2012) 30–37.
[19] T. Chang, S. Cho, J. Kim, J. Schoenleber, C. Frantz, N. Stein, C. Boulanger, W. Lee, Individual thermoelectric properties of electrodeposited bismuth telluride nanowires in polycarbonate membranes, Electrochim. Acta 161 (2015) 403–407.
[20] C. Rodríguez-Fernández, C.V. Manzano, A.H. Romero, J. Martín, M. Martín-González, M.M. de Lima Jr, A. Cantarero, The fingerprint of Te-rich and stoichiometric Bi2Te3 nanowires by Raman spectroscopy, Nanotechnology 27 (7) (2016) 075706.
[21] M.M. Rojo, S. Grauby, J.-M. Rampnoux, O. Caballero-Calero, M. Martin-Gonzalez, S. Dilhaire, Fabrication of Bi_2Te_3 nanowire arrays and thermal conductivity measurement by 3ω-scanning thermal microscopy, J. Appl. Phys. 113 (5) (2013) 054308.
[22] C.V. Manzano, M.N. Polyakov, J. Maiz, M.H. Aguirre, X. Maeder, M. Martín-González, Pulsed current-voltage electrodeposition of stoichiometric Bi2Te3 nanowires and their crystallographic characterization by transmission electron backscatter diffraction, Sci. Technol. Adv. Mater. 20 (1) (2019) 1022–1030.

[23] M.M. Rojo, B. Abad, C. Manzano, P. Torres, X. Cartoixà, F. Alvarez, M.M. Gonzalez, Thermal conductivity of Bi 2 Te 3 nanowires: how size affects phonon scattering, Nanoscale 9 (20) (2017) 6741–6747.
[24] M.M. Rojo, Y. Zhang, C.V. Manzano, R. Alvaro, J. Gooth, M. Salmeron, M. Martin-Gonzalez, Spatial potential ripples of azimuthal surface modes in topological insulator Bi 2 Te 3 nanowires, Sci. Rep. 6 (1) (2016) 1–8.
[25] C.V. Manzano, M. Martin-Gonzalez, Electrodeposition of V-VI nanowires and their thermoelectric properties, Front. Chem. 7 (1) (2019) 516.
[26] J. Martín, M. Martín-González, J. Francisco Fernández, O. Caballero-Calero, Ordered three-dimensional interconnected nanoarchitectures in anodic porous alumina, Nat. Commun. 5 (1) (2014) 5130.
[27] A. Ruiz-Clavijo, Y. Tsurimaki, O. Caballero-Calero, G. Ni, G. Chen, S.V. Boriskina, M. Martín-González, Engineering a full gamut of structural colors in all-dielectric mesoporous network metamaterials, ACS Photonics 5 (2018) 2120–2128.
[28] A. Ruiz-Clavijo, O. Caballero-Calero, M. Martín-González, Three-dimensional Bi_2Te_3 networks of interconnected nanowires: synthesis and optimization, Nanomaterials 8 (5) (2018) 345.
[29] A. Ruiz-Clavijo, O. Caballero-Calero, C.V. Manzano, X. Maeder, A. Beardo, X. Cartoixa, F.X. Álvarez, M. Martín-González, 3D Bi2Te3 interconnected nanowire networks to increase thermoelectric efficiency, ACS Appl. Energy Mater. 4 (2021) 13556–13566.
[30] O. Caballero-Calero, A. Ruiz-Clavijo, C.V. Manzano, M. Martín-González, G. Armelles, Plasmon resonances in 1D nanowire arrays and 3D nanowire networks of topological insulators and metals, Nanomaterials 13 (1) (2023) 154.
[31] A. Ruiz-Clavijo, N. Pérez, O. Caballero-Calero, J. Blanco, F. Peiró, S. Plana-Ruiz, M. López-Haro, K. Nielsch, M. Martín-González, Localization and directionality of surface transport in Bi2Te3 ordered 3D nanonetworks, ACS Nano 17 (17) (2023) 16960–16967.
[32] Z. Tabaie, A. Omidvar, Human body heat-driven thermoelectric generators as a sustainable power supply for wearable electronic devices: recent advances, challenges, and future perspectives, Heliyon (2023) e14707.
[33] J. He, K. Li, L. Jia, Y. Zhu, H. Zhang, J. Linghu, Advances in the applications of thermoelectric generators, Appl. Therm. Eng. (2023) 121813.
[34] J. Liu, Q. Liu, S. Lin, M.Y. Leung, Y. Ma, X. Tao, Wearable thermoelectric generators: materials, structures, fabrications, and applications, Phys. Status Solidi Rapid Res. Lett. 17 (7) (2023) 2200502.
[35] Q. Zhang, K. Deng, L. Wilkens, H. Reith, K. Nielsch, Micro-thermoelectric devices, Nature Electronics 5 (6) (2022) 333–347.
[36] G.-P. Cui, C.-P. Feng, S.-C. Xu, K.-Y. Sun, J.-C. Ji, L. Hou, H.-B. Lan, H.-J. Shang, F.-Z. Ding, 3D-printed Bi2Te3-based thermoelectric generators for energy harvesting and temperature response, ACS Appl. Mater. Interfaces (2024).
[37] A. Amin, R. Huang, D. Newbrook, V. Sethi, S. Yong, S. Beeby, I. Nandhakumar, Screen-printed bismuth telluride nanostructured composites for flexible thermoelectric applications, J. Phys.: Energy 4 (2) (2022) 024003.
[38] Z. Wang, W. Cui, H. Yuan, X. Kang, Z. Zheng, W. Qiu, Q. Hu, J. Tang, X. Cui, Direct ink writing of Bi2Te3-based thermoelectric materials induced by rheological design, Mater. Today Energy 31 (2023) 101206.
[39] A. Sarbajna, A.G. Rösch, L. Franke, U. Lemmer, M.M. Mallick, Inorganic-based printed thermoelectric materials and devices, Adv. Eng. Mater. 25 (2) (2023) 2200980.
[40] C. Hollar, Z. Lin, M. Kongara, T. Varghese, C. Karthik, J. Schimpf, J. Eixenberger, P.H. Davis, Y. Wu, X. Duan, High-performance flexible bismuth telluride thin film from solution processed colloidal nanoplates, Advanced materials technologies 5 (11) (2020) 2000600.
[41] F. Amirghasemi, S. Kassegne, Effects of RF magnetron sputtering deposition power on crystallinity and thermoelectric properties of antimony telluride and bismuth telluride thin films on flexible substrates, J. Electron. Mater. 50 (2021) 2190–2198.
[42] V. Russo, A. Bailini, M. Zamboni, M. Passoni, C. Conti, C. Casari, A. Li Bassi, C. Bottani, Raman spectroscopy of Bi-Te thin films, J. Raman Spectrosc. 39 (2) (2008) 205–210.
[43] Y. Du, G. Qiu, Y. Wang, M. Si, X. Xu, W. Wu, P.D. Ye, One-dimensional van der Waals material tellurium: Raman spectroscopy under strain and magneto-transport, Nano Lett. 17 (6) (2017) 3965–3973.
[44] A. Pine, G. Dresselhaus, Raman spectra and lattice dynamics of tellurium, Phys. Rev. B 4 (2) (1971) 356.
[45] C.V. Manzano, B. Abad, M.M. Rojo, Y.R. Koh, S.L. Hodson, A.M.L. Martinez, X. Xu, A. Shakouri, T.D. Sands, T. Borca-Tasciuc, Anisotropic effects on the thermoelectric properties of highly oriented electrodeposited Bi 2 Te 3 films, Sci. Rep. 6 (2016) 19129.
[46] J. Na, Y. Kim, T. Park, C. Park, E. Kim, Preparation of bismuth telluride films with high thermoelectric power factor, ACS Appl. Mater. Interfaces 8 (47) (2016) 32392–32400.
[47] K. Cicvarić, L. Meng, D.W. Newbrook, R. Huang, S. Ye, W. Zhang, A.L. Hector, G. Reid, P.N. Bartlett, C.K. de Groot, Thermoelectric properties of bismuth telluride thin films electrodeposited from a nonaqueous solution, ACS Omega 5 (24) (2020) 14679–14688.